ELSEVIER

Journal of Microbiological Methods 46 (2001) 193–208

Journal of Microbiological Methods

www.elsevier.com/locate/jmicmeth

Integration of Raman microscopy, differential interference contrast microscopy, and attenuated total reflection Fourier transform infrared spectroscopy to investigate chlorhexidine spatial and temporal distribution in *Candida albicans* biofilms

Peter A. Suci [a,*], Gill G. Geesey [a], Bonnie J. Tyler [b]

[a] *Center for Biofilm Engineering and Microbiology Department, Montana State University, Bozeman, MT 59717-3980, USA*
[b] *Chemical and Fuels Engineering, University of Utah, Salt Lake City, UT 84112, USA*

Received 21 February 2001; received in revised form 3 April 2001; accepted 3 April 2001

Abstract

Two spectroscopic techniques, attenuated total reflection Fourier transform infrared spectroscopy (ATR-FTIR) and Raman microscopy (RM), were used to characterize transport of chlorhexidine digluconate (CHG) in *Candida albicans* (CA) biofilms. Different (volumetric) regions of the biofilm are sampled by these two vibrational spectroscopies making them complementary techniques. Simple mathematical models were developed to analyze ATR-FTIR and RM data to obtain an effective diffusion coefficient describing transport through CA biofilms. CA biofilms were composed primarily of yeast and hyphal forms, with some pseudohyphae. Upper regions of biofilms that had become confluent, (i.e., biofilms that completely covered the germanium (Ge) substratum) were composed primarily of a tangled mass of hyphae with openings between germtubes about 10 to 50 μm across. Quantitative analysis of ATR-FTIR kinetic data curves indicated that the effective diffusion coefficient for transport of CHG through confluent biofilms about 200-μm thick was reduced 0.1 to 0.3 times compared to the diffusion coefficient for CHG in water. Effective diffusion coefficients obtained from analysis of RM data were consistently higher than those indicated by ATR-FTIR data suggesting that transport is more hindered in regions near the base of the biofilm than in the outer layers. Analysis of both ATR-FTIR and RM data obtained from thicker films indicated that adsorption of CHG to biofilm components was responsible for a substantial portion of the transport limitation imposed by the biofilm. Comparison of ATR-FTIR and RM data for both types of biofilms indicated that sites of CHG adsorption were more concentrated in the interfacial region than in the bulk biofilm. Comparison of results for ATR-FTIR and RM measurements suggests that these relatively thick CA biofilms can be modeled, for purposes of predicting transport, approximately as a homogeneous thin planar sheet. Thus, these biofilms offer a relatively tractable model system for initial investigations of the relation between antimicrobial transport and kinetics of antimicrobial action. © 2001 Published by Elsevier Science B.V.

Keywords: Raman microscopy; ATR-FTIR; *Candida albicans*

* Corresponding author.

0167-7012/01/$ - see front matter © 2001 Published by Elsevier Science B.V.
PII: S0167-7012(01)00268-8

1. Introduction

Microbes associated with a surface, generally referred to as a biofilm, typically develop into a densely packed community of cells interconnected by a biopolymeric matrix. Interaction with cellular and matrix components reduce rates of transport of substances in biofilms. Anaerobic microenvironments in dental plaque that enable putative pathogens of periodontal disease to survive (Listgarten, 1994), and biological corrosion cells thought to be responsible for microbial influenced corrosion (Costerton and Boivin, 1987) are examples of the consequences of limited transport that leads to establishment of chemical gradients within the biofilm. Transport of antimicrobial agents (AA), introduced into the bulk aqueous phase, is hindered to portions of at least some biofilms by binding to biofilm components, partitioning into cells and/or being degraded or inactivated by extracellular enzymes (Dibdin et al., 1996; Dunne et al., 1993, Gordon et al., 1991; Nichols et al., 1989). The importance of these delays in exposure of portions of biofilms to the cidal dose of AA, in terms of enhancing the survival potential of biofilm microbes, has not been determined.

A variety of techniques have been used to characterize transport of substances in biofilms (Bryers and Drummond, 1998; Chen and Stewart, 1996; De Beer et al., 1997; Robinson et al., 1997). If the compound of interest is fluorescent, a technique that exploits this property is probably superior to any other due to the inherent sensitivity and possibility of making measurements in situ in real time. Many AA of interest are only weakly fluorescent or have excitation or emission ranges that preclude using a given fluorescence technique. Transport rates of a fluorescent analogue molecule, having approximately the same size, may differ from those of the original AA since functional group chemistry can determine adsorption and partition coefficients.

Vibrational spectroscopies probe quantum state transitions associated with molecular vibrations. In general, they are less sensitive than fluorescence spectroscopies. However, they have the advantage that any organic molecule will produce a spectrum having essentially unique, complex features enabling positive identification. A methodology exploiting attenuated total reflection Fourier transform infrared spectroscopy (ATR-FTIR) was developed previously to measure transport of AA in biofilms (Suci et al., 1994). Raman microscopy (RM) is introduced here as a complimentary technique that can furnish information about the spatial and temporal distribution of AA in the biofilm.

ATR-FTIR is a surface-sensitive technique that measures the kinetics of appearance of AA at the base of the biofilm, i.e., within less than a micron of the substratum/biofilm interface. The signal is collected from the entire area of the interfacial region. Thus, it provides no lateral discrimination. The imaging capability of RM provides lateral discrimination in the plane of the substratum at the micron level. Using conventional optics (i.e., not optics designed to enhance confocality), the sampling volume in the direction perpendicular to the substratum typically extends for a distance substantially greater than a micron. For experiments presented here, this distance was comparable to the thickness of the biofilm.

Candida species are opportunistic pathogens. Associated infections are found in a wide variety of locations in the human body depending on the predisposing condition (Odds, 1988). The rationale for in vitro studies of *Candida albicans* biofilm recalcitrance to AA, due to this organism's involvement in nosocomial infections, has been expressed in a recent publication (Baillie and Douglas, 1998). More generally, even classical infections (e.g., thrush) manifest as a complex biofilm comprised of yeast, hyphae and desquamated epithelial cells. In vitro studies have demonstrated that chlorhexidine may be an effective treatment for oral candidosis (Giuliana et al., 1997; MacNeill et al., 1997). Understanding which factors limit chlorhexidine efficacy toward biofilms should enhance interpretation of clinical results.

2. Materials and methods

2.1. Organisms

C. albicans (CA-1) (Han et al., 1998) is a clinical isolate obtained from the culture collection of Dr. Diane Brawner (Microbiology Department, Montana State University). ATTC24433 (*C. albicans*) was obtained from the culture collection of Dr. James Cutler (Microbiology Department).

2.2. Growth medium

Medium for batch cultures was (per liter): 50 g glucose, 10 g Bacto-Peptone (Difco), and 6 g yeast extract (Difco). Medium for biofilm growth was (per liter): 0.05 g glucose, 0.1 g Bacto-peptone and 0.03 g yeast extract (pH 6.5). Cells were suspended in 0.01 M phosphate buffered saline (PBS) to encourage initial attachment to the substratum. PBS was (per liter): 0.34 g monobasic sodium phosphate, 2.56 g dibasic sodium phosphate and 8.50 g NaCl (pH 7.2).

2.3. Flow system

The flow system was similar to that described (Vrany et al., 1997), except that inoculation of the biofilm (seeding of the substratum) was from a cell suspension in PBS instead of from a continuous culture. The flow cell has been described (Suci et al., 1997). The flow channel is approximately rectangular ($45 \times 10 \times 0.86$ mm) with entrance and exit ports at each end of the long dimension. The top and bottom walls of the flow channel are comprised of a window for microscopic observation made from a coverslip and the internal reflection element (IRE). The IRE was a single crystal, trapezoidal germanium (Ge) prism (Harrick Scientific, Ossining, NY) ($50 \times 20 \times 2$ mm^3, 45°). The thin walls of the flow cell cavity are composed of a sandwich of teflon and viton spacers. The teflon spacer contacts the IRE. For biofilm culturing, the entire flow system was placed in an incubator at 37°C. Flow rate was maintained at 0.5 ml/min by making necessary adjustments in the pump rotation speed with drop counts per time in flow break tubes (calibrated by determination of the volume of liquid per drop) used as feedback.

2.4. Surface preparation

The surface of the IRE was cleaned by a protocol described, except that there was no final rinse with dichloromethane (Frølund et al., 1996).

2.5. Biofilm inoculum and culturing

A batch culture (100 ml), inoculated from a slant, was grown overnight at 37°C with shaking at 160 rpm. A fresh batch culture (100 ml) was inoculated with 3 ml of the first batch culture. In early stationary phase (approximately 10 h after inoculation), 1 ml of the culture was spun down and resuspended in PBS. A 100 μl of this cell suspension (containing approximately 2×10^8 cells/ml) was added to 35 ml of PBS in a flask connected to the autoclave-sterilized flow system described. This dilute PBS cell suspension was pumped through the flow cell for 30 min at 0.5 ml/min. The surface of the IRE was then viewed at 200× and two images acquired. Cell counts on the surface were between 1.24 and 3.29 ($\times 10^5$/cm^2) for all experiments. Biofilms were cultured for approximately 16 h at 37°C.

2.6. Dosing with chlorhexidine

Appropriate dilutions were made of a 20% solution of chlorhexidine digluconate (CHG). CHG in (biofilm) culture medium was introduced into the flow cells by diverting the flow at the teflon valve located proximal to the flow cell entrance port. Rinsing was initiated by diverting the flow back to pure culture medium using the same valve. The period during which CHG was diverted into the flow cell is referred to as the dosing period. CHG dosing was at 0.2% for ATR-FTIR measurements and 5% for RM measurements.

2.7. ATR-FTIR

During the course of dosing with CHG and subsequent rinsing infrared (IR), spectra were acquired during 1-min intervals using a Nicolet 740 Fourier transform infrared (FTIR) spectrometer equipped with an ATR mirror assembly (Harrick Scientific). Details pertaining to IR spectroscopy were described (Suci and Geesey, 2000).

2.8. Microscope

The microscope was an Olympus BX60. Differential interference contrast (DIC) optics were used to visualize biofilms using either a 20× (Olympus, UPlanFl 20×/0.50) or a 40× water immersion (Olympus, LUMPlanFl 40×/0.8 W) objective. A black and white Photometrics CCD camera was used to digitally capture the images, which were analyzed using Media Cybernetics Image-Pro Plus software.

2.9. Raman imaging system

The main components of the Raman imaging system (ChemIcon, Pittsburgh, PA) are the microscope described above, a 2-W 532-nm laser coupled to the microscope with a fiber optic cable and beam couplers, a liquid crystal tunable filter (Split Evans Design) for frequency discrimination, a CCD camera and Chemimage V2.0 visualization and processing software. All Raman images were acquired with the $40\times$ water immersion lens. The instrument is essentially the same as one described (Morris et al., 1999), except that laser plasma lines are excluded by rejection filters instead of holographic notch filters.

2.10. Estimation of biofilm thickness and surface coverage

Thickness of the biofilms was estimated by taking the difference in the vernier caliper reading between the position of the substratum and cells (mostly hyphae) at the top of the biofilm (biofilm/bulk-liquid interface). The position of the substratum was determined by finding a location for which a scratch was visible and then bringing the scratch into focus. These locations were quite rare in confluent biofilms. Thickness used to analyze ATR-FTIR data was based on measurements at three locations, except for one experiment (experiment 3 referred to below), which was based on nine locations. Thickness used to analyze RM measurements was evaluated by finding a location at which the position of the substratum could be determined that was as close as possible to the RM sampling location (approximately the middle of the flow cell). Thickness estimations were performed at $400\times$. With the focus on the top of the biofilm at one location, it was possible to move the field of view around in the plane of the substratum, while retaining a focused image of the top of the biofilm, giving the impression that the biofilm could be approximated as a planar sheet.

Confluent biofilms exhibited no regions where the Ge surface was completely free of cells. Data was collected from a number of biofilms that were not confluent. These biofilms displayed regions of varying size that were practically free of cells. Colonized regions were not as thick as confluent biofilms. Data from the biofilm having almost complete surface coverage is presented here (experiment 5). Biofilm surface coverage was estimated by visualizing the biofilms using DIC microscopy. Surface coverage was estimated from five images acquired from randomly located fields (465×300 μm^2) at $200\times$ using the image analysis software with pixel brightness as the criterion for distinguishing colonized (dark) and cell-free areas (light). The Ge surface is quite reflective and provides a high contrast background for visualization of cells.

2.11. ATR-FTIR and RM data acquisition

Use of ATR-FTIR difference spectra to follow appearance of AA in the substratum interfacial region has been described previously (Suci et al., 1994, 1998; Vrany et al., 1997).

Raman images were acquired at 1.5 W laser power. The 512×512 CCD array was binned 50×50 during collection resulting in a 10×10 array of pixels. With this binning, each pixel has a dimension of 10×10 μm^2 in the plane of the substratum. Although the term voxel was introduced to refer to volume elements, pixel seems adequate for purposes here. Acquisition time was 1 s per wavelength. For CHG measurement, images were collected for wavelengths between 580.6 and 582.6 nm at 0.1-nm intervals (1573.4 to 1629.6 cm^{-1}). It required 59 s to obtain the composite image composed of each of the 20 images obtained at each wavelength. Due to non-uniform laser intensity, spectra collected from pixels in the more central region of the image delineated by the CCD array (approximately 100×100 μm^2 total size at $400\times$) provided more information about CHG concentration than those on the periphery.

Areas of spectral features for both ATR-FTIR and RM data were computed for the region bounded by the data points and a linear baseline drawn between the two limits of the integration (baseline-subtracted areas). Band areas are presented as unit-less quantities. Both ATR-FTIR and RM data were imported into GRAMS/386 software for spectral manipulation and analysis (Galactic Industries, Salem, NH). Area calculations for RM data were made on spectra that had wavelength in units of nm, since this avoids an importing inconvenience. The software supplied by the manufacturer allows imaging using pixel

brightness only. For the present application, this provides little, if any, information on CHG concentration, since differences in pixel brightness due to signal originating from CHG are overwhelmed by large differences in the baseline: a relatively large signal that is fairly constant across the frequency range of the measurement. Thus, baseline-subtracted areas must be computed to obtain quantities that correlate with CHG concentration.

For some experiments, both ATR-FTIR and RM measurements were acquired from the same biofilm. These measurements were performed sequentially by first shuttling the flow system between instruments.

2.12. Sampling volumes of ATR-FTIR and RM

The evanescent field that samples the interfacial region in ATR-FTIR has been well-characterized (Knutzen and Lyman, 1985). The theoretical intensity of the evanescent field versus distance from the substratum surface is plotted in Fig. 1a for the wavenumber corresponding to the maximum of the CHG band used to follow CHG transport using ATR-FTIR (see Fig. 2a). The evanescent field is produced by multiple total reflections of the IR beam within the IRE, a trapezoidal Ge prism. The sampling area is constrained in the lengthwise direction by the spacers that serve as the walls of the cavity of the flow cell. In the widthwise direction, the sampling area is constrained by the beam width which is approximately 6 mm. In short, the ATR-FTIR yields

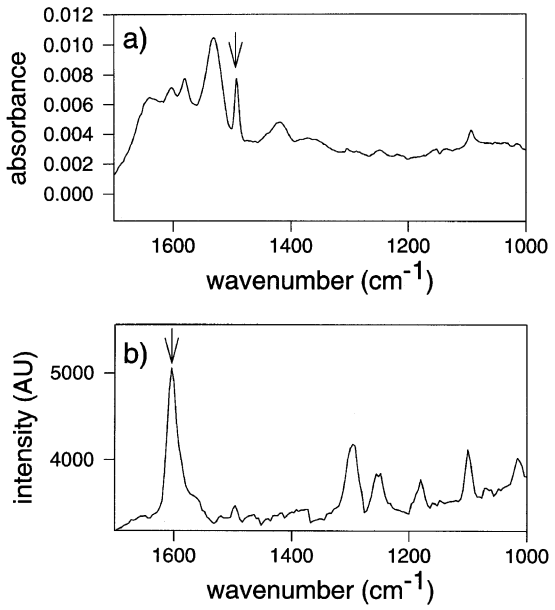


Fig. 2. (a) ATR-FTIR spectrum of 2% CHG. Area of the band indicated (1479–1501 cm^{-1}), originating from vibrational modes associated with the chlorophenyl groups, was used to follow transport to the Ge substratum. (b) Raman spectrum of CHG, condensed by drying a 20-μl drop of 5% CHG on the surface of a Ge prism. Area of the band indicated (1585–1626 cm^{-1}), originating from the guanidine groups, was used to follow transport.

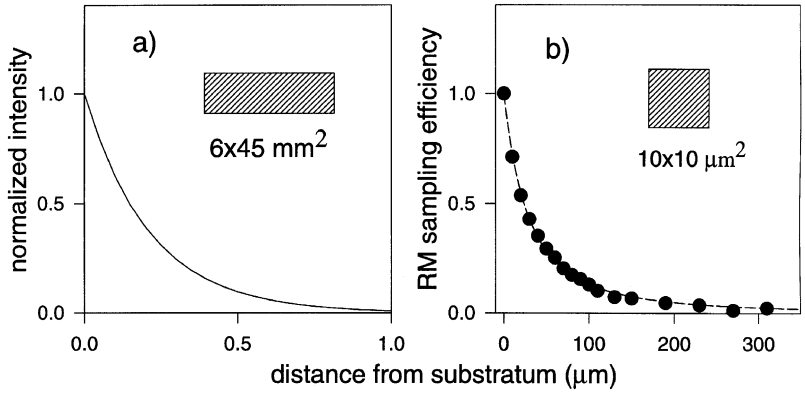


Fig. 1. Sampling volumes of (a) ATR-FTIR and (b) RM. (a) Theoretical curve describing the intensity of the IR evanescent field at 1493 cm^{-1} (CHG band in Fig. 2) versus distance. (b) Ge signal measured from a planar Ge surface with a 40 × objective normalized to 1 (filled circles), fit with an inverse squared function (broken line) versus distance. Penetration depth is 0.213 μm for the evanescent field (ATR-FTIR). An equivalent proportion of the signal (63%) detected by the RM originates from within 71 μm of the surface. Inserts indicate cross-section of the sampling volume (lateral area) for each instrument.

information from a relatively large lateral area (6×45 mm^2) located quite near the interface (< 1 μm). This sampling region is referred to as the evanescent volume.

The effective sampling volume of RM is constrained by the S/N ratio and the sensitivity to CHG. For these experiments the lateral dimensions of the sampling volume (i.e., dimensions in the plane of the interface) were 10×10 μm^2. RM sampling efficiency in the direction perpendicular to the plane of the substratum was estimated for the $40\times$ objective by acquiring the signal from a sterile, clean IRE placed in the flow cell, filled with water. The result of measuring the Raman signal from the Ge band at 300 cm^{-1} versus distance from the plane of focus is shown in Fig. 1b. The curve is fit adequately ($r^2 = 0.999$) by an inverse squared function:

$$\text{band area}_{\text{Ge}} = C\left(1/(d-k)^2\right) \quad (1)$$

where d is distance from the plane of focus and C and k are found by a least squares fit ($k = 57$ μm). In short, with the focus at the substratum, the RM sampling volume is a region that is relatively long and thin with the long axis perpendicular to the plane of interface and a sampling efficiency that decreases approximately as the inverse square of the distance from the substratum. All RM measurements were performed with the vernier caliper reading set for focus at the substratum.

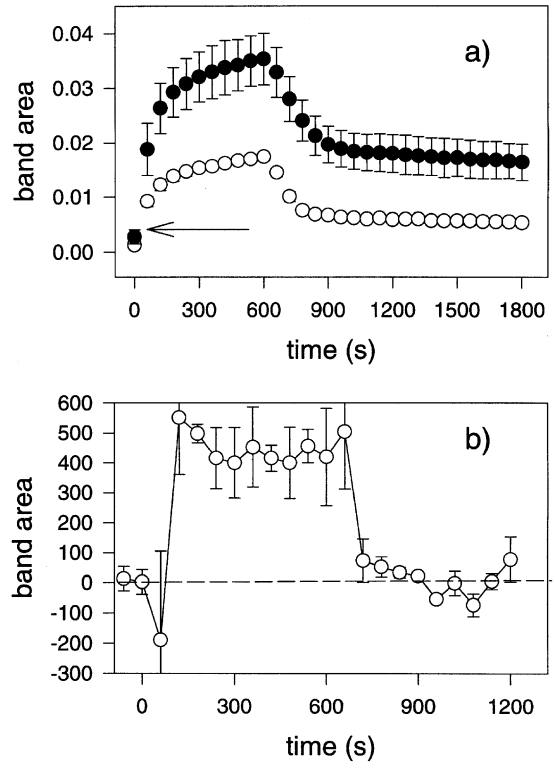


Fig. 3. Transport of CHG into sampling volume for sterile IRE (no biofilm). Points and error bars are means and standard deviations for three data sets. (a) ATR-FTIR data curve (0.2% dosing concentration in water); unconditioned surface (open circles); conditioned surface (closed circles). IR signal expected from 0.2% bulk CHG solution with no adsorption in the interfacial region is indicated by the arrow. (b) Raman data curve (5% dosing concentration).

2.13. Calibration using a sterile IRE

Fig. 2 shows IR and Raman spectra of CHG and indicates the bands used to follow temporal changes in CHG concentration. Fig. 3 shows ATR-FTIR (a) and RM (b) (kinetic) data curves for a sterile, clean IRE (no biofilm). These are constructed by plotting band area versus time and are referred to as simply ATR-FTIR or RM data curves. In each case, dosing was for 10 min (dosing period) followed by a rinse period. CHG dosing was at 0.2% (ATR-FTIR) or 5% (RM). Data presented in Fig. 3 are actually mean data curves: data are means and standard deviations for three repetitions. For ATR-FTIR measurements, the background spectrum was acquired immediately before CHG was diverted into the flow cell. The ATR-FTIR data curve in Fig. 3a rises above the signal expected from 0.2% CHG (the dosing level), indicating that a substantial amount of CHG adsorbed to the Ge substratum. The ATR-FTIR data curves in Fig. 3a were acquired for CHG in water (not culture medium). Exposing the Ge substratum to culture medium for 30 min (i.e., conditioning with culture medium) increases the amount of CHG adsorbed in the interfacial region at the end of the rinsing period by a factor of about 3, compared to an unconditioned Ge substratum. RM data was acquired from the pixel that appeared most bright in the unprocessed images. The mean of the three Raman data curves is negative at 1 min. All RM data curves exhibit a relatively large negative signal (band area)

at an early time point that corresponds to the time expected for the CHG front to sweep across the field of view. The spectra for this time point exhibit a pronounced sloping baseline. This data pair in RM data curves was set to zero (band area) at time zero for purposes of modeling.

Fig. 4 shows ATR-FTIR (a) and RM (b) calibration curves constructed by dosing the flow cell with increasing concentrations of CHG (sterile IRE, no biofilm, unconditioned). The ATR-FTIR data are the signal at the end of the dosing period. Both bulk (solution-phase) CHG and CHG adsorbed to the IRE contribute to the ATR-FTIR signal. At higher bulk concentrations, the binding sites approach saturation. Thus, the curve is fairly linear for concentrations above 0.5% ($r^2 = 0.998$). The slope of this portion of the curve was used to estimate the ATR-FTIR signal expected from a 0.2% bulk CHG solution (i.e., with no adsorption to the interface). RM data (Fig. 4b) are means of five data points in the plateau region of a data curve acquired at each CHG concentration (time 5 to 10 min during dosing). The entire RM data set in Fig. 4b was acquired at one location. Although our instrument is able to discriminate 1% CHG from background noise, the percent standard deviation for this concentration is quite high. The linear relation between the RM signal and the CHG concentration is quite good within one experiment (i.e., for a series of measurements taken in sequence at one location). Between experiment correlation between RM signal and CHG concentration is not as good (slope = 77 (SD = 12); intercept = 18 (SD = 25); $r^2 = 0.8518$) (data not shown). This poorer correlation may be due to differences in laser intensity distribution across the collection area between experiments.

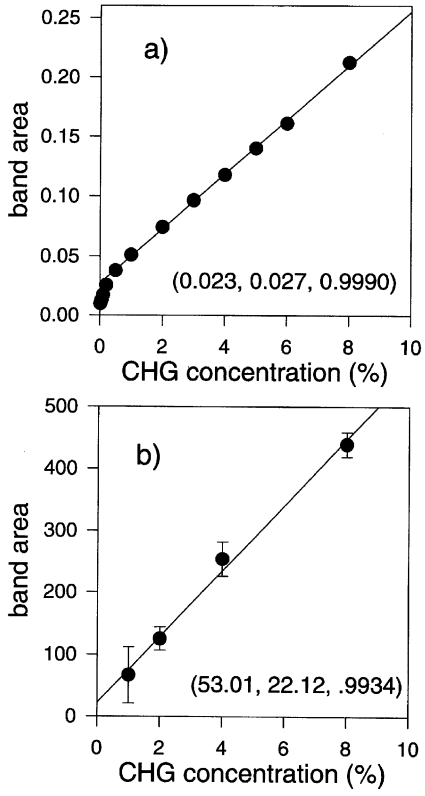


Fig. 4. Dosing concentration of CHG in the flow cell versus band area: (a) ATR-FTIR and (b) Raman. For each data set the slope, intercept and R^2 of the regression line are indicated in brackets; for (a) data for dosing concentrations 0.5% and above were used for the regression since at these higher concentrations the adsorption binding curve approaches saturation (see text). Error bars in (b) are standard deviations for five data points acquired in the plateau region of the dosing portion of the data curve (time 5–10 min).

2.14. Modeling of transport

It was assumed that diffusion of CHG through the biofilm could be described by Fick's law in one dimension:

$$D(\delta^2 C/\delta z^2) = \delta C/\delta t \qquad (2)$$

where D is the diffusion coefficient, C is concentration, z is distance from the substratum in the direction perpendicular to the plane of the interface, and t is time. Effects of hindered transport due to adsorption to biofilm matrix components and partitioning into cells were assumed to result in a decrease in D, so that it can be considered an effective diffusion coefficient (D_e). This approach has been used previously to model transport in biofilms (Nichols et al., 1989).

For modeling of ATR-FTIR data, it was assumed that adsorption to sites in the interfacial region could be described by a simple Langmuir process:

$$\mathrm{d}(C_A)/\mathrm{d}t = k_a(C_{s,tot}C_B) - (k_a C_B + k_d)C_A \qquad (3)$$

where C_A is the (surface) concentration of adsorbed CHG, $C_{s,tot}$ is the density of total adsorption sites (i.e., surface concentration), C_B is concentration of bulk CHG in the interfacial region predicted by Eq. (2), and k_a and k_d are rate constants for adsorption and desorption, respectively.

Initial estimates for $C_{s,tot}$, k_a and k_d were obtained by fitting the latter part of the dosing portion of the data curve fit with an exponential expression:

$$\text{ATR-FTIR signal}(\text{band area}) = c_1(1 - \exp[-c_2 t]) \quad (4)$$

where t is time and c_1 and c_2 are floating parameters. Eq. (4) describes the shape of a theoretical kinetic data curve obtained by measuring accumulation of a substance at an interface where the adsorption process is described by Eq. (3) with bulk concentration held constant. Parameters $C_{s,tot}$, k_a and k_d that appear in Eq. (3) are related to c_1 and c_2 by:

$$k_a = (c_2 - k_d)/C_B \quad (5)$$

$$C_{s,tot} = c_1 c_2 / k_a C_B. \quad (6)$$

For modeling RM data, Eq. (2) was used to predict the CHG concentration throughout the entire biofilm thickness. The derived concentrations for different lamella of the biofilm were then weighted by Eq. (1) in order to account for the RM sampling efficiency perpendicular to the plane of the substratum (Fig. 1b). (i.e., with the vernier caliper reading set for focus at the substratum). The sum of these values and the predicted signal from the bulk volume was used to fit the data. It was assumed that the bulk volume filled within 30 s. This is consistent with RM data curves acquired with a sterile IRE (Fig. 3b). RM sampling of the bulk volume was evaluated as the integral of the sampling efficiency from the biofilm/bulk-liquid interface to infinity.

Eqs. (2) and (3) were evaluated by two software programs developed independently. In the first program, Eq. (2) was evaluated by a truncated infinite series expression (Eq. (4.17), Crank, 1956) and used to calculate the time dependence for appearance of bulk CHG in the interfacial region (Nichols et al., 1989). Eq. (3) was evaluated numerically. Software was written in GRAMS/386 array basic. The second program evaluates both Eqs. (2) and (3) numerically. It is available commercially (AQUASIM, 2.0, Peter Reichert, Computer Systems Sciences Department, EAWAG, Switzerland). Results with simulated data were used to test the consistency between the two programs and allowed checking for user and/or programmer errors. The second program was particularly useful since it allowed modeling of an entire data curve (both dosing and rinsing portions), gave confidence intervals for the fitted parameters, and permitted least-squares-criterion optimization of D_e, k_a, k_d, and $C_{s,tot}$.

3. Results

3.1. Biofilm characteristics

Fig. 5 shows micrographs depicting the stages of *C. albicans* biofilm development. The Ge substratum is first seeded with yeast from a batch culture. A proportion of the attached yeast form microcolonies composed of clusters of yeast cells, pseudohyphae, and hyphae. Hyphae, 50–100 μm in length, typically extend into void regions, along the substratum, from the dense colonies. Hyphae and pseudohyphae are also present in the outer layers of the dense colonies, near the biofilm/bulk-liquid interface. Microcolonies coalesce into a biofilm that eventually covers the substratum completely. Upper regions of confluent biofilms consist primarily of hyphea with openings between germtubes that are approximately 10 to 50 μm across (Fig. 6).

In general, exposure to either 0.2% CHG, 5% CHG or even higher doses (biofilms were exposed to 20% in a preliminary experiment), caused no visible changes in biofilm structure. Induced loss of single cells or larger flocs was not apparent.

3.2. Data analysis

Fig. 7 is a schematic clarifying the terminology used to refer to different regions of the in vitro system.

Fig. 8a and b shows ATR-FTIR data acquired during dosing of a biofilm with 0.2% CHG. The estimated mean biofilm thickness was 187 μm (experiment 3). The shape of the curve described by the data is sigmoidal. This is the approximate shape

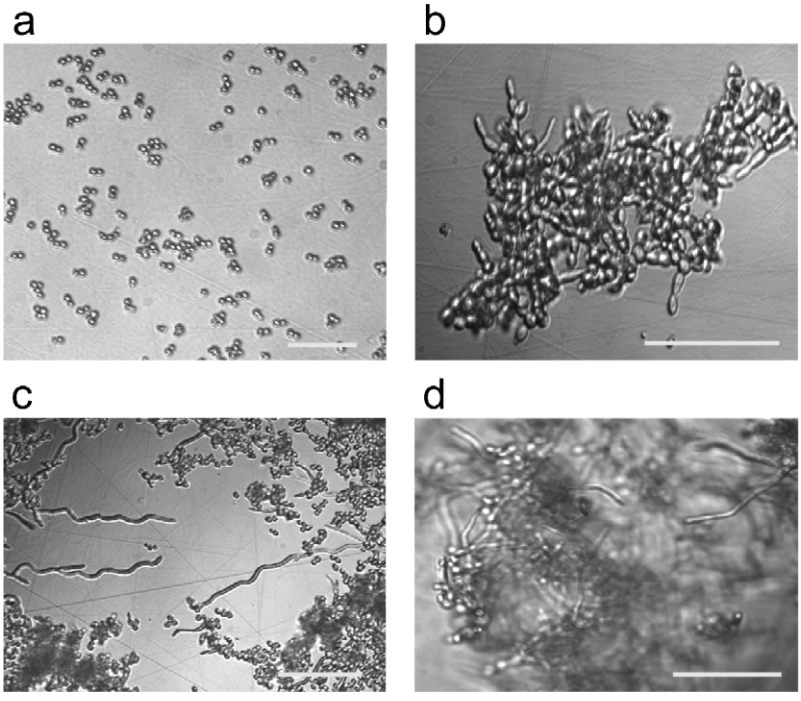


Fig. 5. DIC micrographs of CA biofilms: (a) biofilm is initiated by seeding yeast onto Ge substratum; (b) microcolonies develop exhibiting yeast, pseudohyphal and hyphal forms after approximately 5 h; (c,d) as microcolonies coalesce hyphae grow both into void spaces along substratum (c), and into the bulk volume (d). Bars indicate 50 μm.

predicted for appearance of CHG in the ATR-FTIR evanescent volume via transport by diffusion from the bulk volume through a thin planar sheet or film (Eq. (2)). Fig. 8c shows ATR-FTIR data for both the

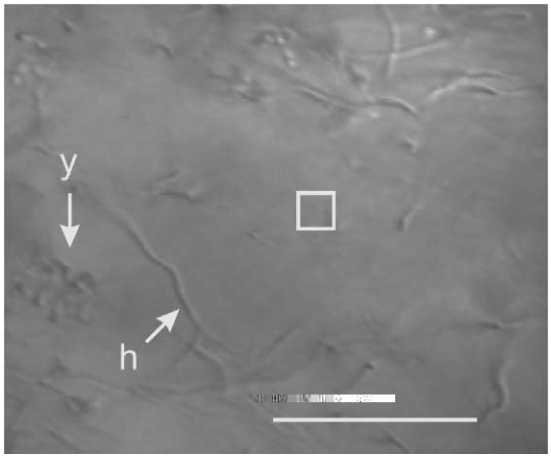


Fig. 6. DIC micrograph of typical region of a confluent CA biofilm (approximately 200 μm thick); focus is 120 μm from the Ge substratum (80 μm into the biofilm); both hyphal (h) and yeast (y) forms can be distinguished. Square indicates pixel size (for RM measurement) and location for this field of view. Bar indicates 50 μm.

Fig. 7. Schematic clarifying terminology used to refer to different regions of the in vitro system. Lower illustration is enlarged view of the region referred to as the interfacial region or evanescent volume, conventionally delineated by its penetration depth (broken line). For simplicity, CHG is shown adsorbing only to the Ge substratum.